

# Unification of plastic compression in a coupled mechanical and water retention model for unsaturated soils

Martí Lloret-Cabot; Simon J. Wheeler and Marcelo Sánchez

## Abstract

Wheeler et al. (2003) presented an elasto-plastic constitutive model for unsaturated soils which represents both mechanical behaviour and water retention behaviour, including the coupling between them. A crucial feature of the model is that the occurrence of plastic compression during all types of stress path is unified as a single process, with plastic compression during loading, plastic compression during wetting (collapse compression) and plastic compression during drying (irreversible shrinkage) all represented by yielding on a single *LC* yield curve. This paper explains how the model is able to predict the possible occurrence of plastic compression during each type of stress path and, in each case, links this to a physical explanation of the process involved. A simulation of an experimental test demonstrates the capability of the model to predict accurately the variation of both void ratio and degree of saturation during successive stages of drying, loading and wetting, where large magnitudes of compression occurred in all three test stages.

*Key words:* constitutive modelling; unsaturated soils;

## Introduction

Experimental evidence from laboratory testing of unsaturated soils indicates that plastic (irreversible) compression can occur during loading paths (increase of net stress), wetting paths (decrease of suction) or drying paths (increase of suction).

The demonstration by Alonso et al. (1987) that plastic compression during loading and plastic compression during wetting (collapse compression) are both essentially the same process and that they can both be interpreted as yielding on a single Loading Collapse (*LC*) yield curve was an enormously significant development in the understanding of unsaturated soil behaviour. It also led to the development of the first elasto-plastic mechanical constitutive model for unsaturated soils, the well-known Barcelona Basic Model or BBM (Alonso et al. 1990). However, in order to also include the possibility of plastic compression during drying paths, Alonso et al. (1990) had to introduce a second yield curve within the BBM, known as the Suction Increase (*SI*) yield curve. The occurrence of plastic compression during drying is therefore treated within the BBM (and many subsequent models) as an essentially different process to plastic compression during loading or wetting. In the BBM, plastic

compression on drying is generally only predicted when the suction exceeds the maximum value previously applied to the soil, and this is inconsistent with experimental behaviour observed in many tests (see Wheeler et al. 2003).

Wheeler et al. (2003) presented a coupled elasto-plastic model for unsaturated soils, which represents both mechanical behaviour and water retention behaviour, including the coupling between them. The model was originally presented solely for isotropic stress states but has subsequently been extended to general stress states (see, for example, Lloret-Cabot et al. 2013). In this model, a single yield curve (the *LC* yield curve) represents the mechanical behaviour, with the occurrence of plastic volumetric strains (and plastic shear strains in the generalised version of the model) being limited to yielding on this curve. Two other yield curves (the *SI* and *SD* yield curves) represent the water retention behaviour, with plastic changes of degree of saturation occurring during yielding on either of these curves. Coupled movements of the three yield curves represent the influence of plastic changes of degree of saturation on mechanical behaviour and the influence of plastic volumetric strains on water retention behaviour.

A crucial feature of the model of Wheeler et al. (2003) is that plastic compression during loading, plastic compression during wetting (collapse compression) and plastic compression during drying (irreversible shrinkage) are all considered as a single process and all are represented by yielding on a single *LC* yield curve. Complete unification of the occurrence of plastic compression, irrespective of the type of stress path, has therefore been achieved. It is clear that this feature has not been fully understood by many of the commentators on the model of Wheeler et al. (2003) and also that some of these commentators have not fully understood how the model predicts the occurrence of plastic volumetric strains during some types of stress path. The aim of this paper is therefore to set out more fully how the model of Wheeler et al. (2003) unifies the occurrence of plastic volumetric strains during all types of stress path as yielding on a single *LC* yield curve, to show how this works for loading, wetting and drying paths, and to demonstrate that this results in accurate modelling of soil behaviour by simulating the soil response in a single experimental test involving all three types of stress path.

## **The constitutive model**

The constitutive model of Wheeler et al. (2003) was developed by considering the roles of “bulk water”

and “meniscus water” within unsaturated soils, where bulk water is the water within those voids that are entirely filled with water and meniscus water bridges are the small amounts of water that remain around those inter-particle contacts (or inter-aggregate contacts) that are surrounded by air-filled voids. Meniscus water bridges provide an additional component of normal contact force, which, because of the frictional nature of these inter-particle or inter-aggregate contacts, makes slippage at the contacts less likely and hence increases the stability of the soil skeleton against mechanical yielding (the onset of plastic volumetric strains or plastic shear strains). The additional stabilising effect provided by meniscus water is predominantly controlled by the number of meniscus water bridges, rather than the value of suction within the meniscus water, because it can be shown that variation of suction within an individual meniscus water bridge has a relatively modest effect on the additional component of normal force. This means that the additional stabilising effect of meniscus water bridges can be related to plastic changes of degree of saturation  $S_r$ , which represent the flooding or emptying of individual voids with water (and hence the loss or gain of meniscus water bridges).

The stress variables used in the model of Wheeler et al. (2003) are the “Bishop’s stress” tensor  $\sigma_{ij}^*$  and the “modified suction”  $s^*$ . For isotropic stress states, the only stress variables required are the mean Bishop’s stress  $p^*$  and the modified suction  $s^*$ , defined as follows:

$$p^* = p - S_r u_w - (1 - S_r) u_a = \bar{p} + S_r s \quad (1)$$

$$s^* = n(u_a - u_w) = ns \quad (2)$$

where  $p$  is the mean total stress,  $u_w$  is the pore water pressure,  $u_a$  is the pore air pressure and  $n$  is the porosity.  $\bar{p}$  and  $s$  are the mean net stress and matric suction respectively (the stress variables used in more conventional constitutive models for unsaturated soils, such as the BBM). The stress variables  $p^*$  and  $s^*$  are work-conjugate with the volumetric strain increment  $d\varepsilon_v$  and the decrement of degree of saturation  $-dS_r$  respectively (see Houlsby 1997). Soil mechanics sign convention is adopted in this paper with compressive stresses and associated contractile strains taken as positive.

The model includes three yield curves: a Loading Collapse (*LC*) yield curve for the mechanical behaviour and Suction Increase (*SI*) and Suction Decrease (*SD*) yield curves for the water retention behaviour. For isotropic stress states, the three yield curve equations are:

$$F_{LC} = p^* - p_0^* = 0 \quad (3)$$

$$F_{SI} = s^* - s_I^* = 0 \quad (4)$$

$$F_{SD} = s_D^* - s^* = 0 \quad (5)$$

where  $p_0^*$ ,  $s_I^*$  and  $s_D^*$  are the hardening parameters defining the locations of the *LC*, *SI* and *SD* yield curves respectively (see Figure 1).

Yielding on the *LC* curve is associated with inter-particle or inter-aggregate slippage and this causes plastic volumetric strain (mechanical behaviour) but no plastic change of degree of saturation. Yielding on *SI* or *SD* curves is associated with emptying or filling of voids with water and this causes plastic changes of degree of saturation (retention behaviour) but no plastic volumetric strains. Note that there is no ambiguity at the intersection between the *LC* and *SD* or *SI* yield curves because the associated flow rules adopted are defined independently: a flow rule associated with yielding on the *LC* yield curve to compute plastic volumetric strain, and a flow rule associated with yielding on the *SD* or *SI* yield curve to compute plastic changes of degree of saturation (see also Lloret-Cabot et al., 2013).

For the mechanical behaviour, the value of mean Bishop's stress required to cause yielding on the *LC* yield curve  $p_0^*$  is increased or decreased if the stabilising effect of meniscus water bridges increases or reduces as a consequence of a plastic change of degree of saturation (corresponding to voids emptying or filling with water and a change in the number of meniscus water bridges). This means that yielding on the *SI* or *SD* yield curves (which produces plastic decreases or increases of degree of saturation respectively) produces coupled outward or inward movements of the *LC* yield curve respectively. For the case of yielding on the *SI* or *SD* curve alone (no simultaneous yielding on the *LC* curve), this coupled movement of the *LC* curve is given by:

$$\frac{dp_0^*}{p_0^*} = k_l \frac{ds_I^*}{s_I^*} = k_l \frac{ds_D^*}{s_D^*} \quad (6)$$

where  $k_l$  is a coupling parameter.

Similarly, for the water retention behaviour, the value of modified suction required to cause yielding on the *SI* or *SD* curve ( $s_I^*$  or  $s_D^*$  respectively) is increased by any plastic volumetric strain (this

represents the influence on water retention behaviour of any decreases in the dimensions of voids and of the connecting passageways between voids). This means that yielding on the *LC* yield curve (which produces plastic volumetric strain) produces coupled upward movements of the *SI* and *SD* yield curves. For the case of yielding on the *LC* curve alone (no simultaneous yielding on the *SI* or *SD* curve), these coupled movements of the *SI* and *SD* curves are given by:

$$\frac{ds_D^*}{s_D^*} = \frac{ds_I^*}{s_I^*} = k_2 \frac{dp_0^*}{p_0^*} \quad (7)$$

where  $k_2$  is a second coupling parameter.

In the general case of simultaneous yielding on two yield curves, the overall movement of the *LC* yield curve is the result of a combination of two components: a direct one (due to any yielding on the *LC* curve itself) and a coupled one (due to any plastic change of degree of saturation). The sum of these two components of movement governs the variation of the location of the *LC* yield curve and results in the following hardening rule:

$$dp_0^* = p_0^* \left[ \frac{vd\varepsilon_v^p}{\lambda - \kappa} - \frac{k_1 dS_r^p}{\lambda_s - \kappa_s} \right] \quad (8)$$

Similarly, overall movements of the *SD* and *SI* yield curves for simultaneous yielding are the result of two components: a direct one (due to any yielding on *SD* or *SI*) and a coupled one (due to any plastic volumetric strain). The sum of these two components of movement governs the variation of the location of the *SD* or *SI* yield curves and results in the second hardening rule:

$$ds_\beta^* = s_\beta^* \left[ -\frac{dS_r^p}{\lambda_s - \kappa_s} + k_2 \frac{vd\varepsilon_v^p}{\lambda - \kappa} \right] \quad \beta = SI / SD \quad (9)$$

Note that when yielding on the *LC* curve alone takes place, the movement of the *LC* curve is governed by Equation 8 but with  $dS_r^p$  equal to 0. Similarly, the hardening rule associated with yielding on the *SD* or *SI* curve alone is given by Equation 9 with  $d\varepsilon_v^p$  equal to 0. The full set of equations describing the model for isotropic stress states is given in Wheeler et al. (2003), with extension to general stress states given in Lloret-Cabot et al. (2013).

## Prediction of plastic compression during loading, drying or wetting

Figure 2 shows examples of loading, drying and wetting paths where the model of Wheeler et al. (2003) would predict occurrence of plastic volumetric strains. All stress paths are plotted in the  $s^*:p^*$  plane and, in all cases, the initial locations of the *LC*, *SI* and *SD* yield curves are represented by solid lines, the final positions of the yield curves are indicated by dashed lines and an initial stress state that is inside all three yield curves is assumed.

Stress path *AB* represents a conventional isotropic loading test, where mean net stress  $\bar{p}$  is increased at constant suction  $s$ . As  $\bar{p}$  is increased there is a significant increase of mean Bishop's stress  $p^*$  (see Equation 1) and also a modest decrease of modified suction  $s^*$  (see Equation 2), because of the reduction of porosity  $n$  predicted during loading. Elastic volumetric strains are predicted throughout loading path *AB*, because of the increase of  $p^*$ . Plastic volumetric strains commence at the yield point  $Y_1$ , as the stress path reaches the *LC* yield curve. On completion of the loading path *AB*, the *LC* yield curve has been pushed outwards and there have also been a coupled upward movements of the *SI* and *SD* yield curves (see Equation 7). These coupled movements of the *SI* and *SD* curves are not associated with any occurrence of plastic changes of degree of saturation, because (in the example shown) the stress path has not actually reached the *SI* or *SD* curve.

Stress path *CD* represents a conventional drying test under an isotropic stress state, where suction  $s$  is increased at constant mean net stress  $\bar{p}$ . As  $s$  is increased there is a significant increase of modified suction  $s^*$  (see Equation 2), but there is also a significant increase of mean Bishop's stress  $p^*$  (see Equation 1), due to the increase in value of the product  $S_r s$ . Again, elastic volumetric strains are predicted throughout drying path *CD* (due to the increase of  $p^*$ ), and plastic volumetric strains are predicted from yield point  $Y_2$ , when the stress path reaches the *LC* yield curve. On completion of the drying path *CD*, the *LC* yield curve has been pushed outwards and there have also been coupled upward movements of the *SI* and *SD* yield curves. It is important to note that plastic compression during drying is caused by the increase of mean Bishop's stress  $p^*$ , and it is associated with the decrease of pore water pressure  $u_w$  within voids filled with bulk water. Drying-induced plastic compression generally occurs when the drying is not causing plastic decreases of degree of saturation  $S_r$  (i.e. when the *SI* yield curve has not been reached), because this would be associated with an

increased number of contacts affected by meniscus water bridges and hence increased stability of the soil skeleton (in the model this would be represented by coupled outward movement of the  $LC$  yield curve, which would take the  $LC$  curve away from the stress point).

Stress path  $EF$  represents a conventional wetting test under an isotropic stress state, where suction  $s$  is reduced at constant mean net stress  $\bar{p}$ , leading to significant decrease of  $s^*$  (Equation 2) and significant decrease of  $p^*$  (Equation 1). Negative elastic volumetric strains are predicted throughout wetting path  $EF$ , due to the decrease of  $p^*$ . This represents wetting-induced swelling. During the initial elastic section of the stress path, the reduction of  $p^*$  means that the stress path is moving away from the  $LC$  yield curve. However, the  $SD$  yield curve is reached at yield point  $Y_3$ , and from this point onwards the yielding on the  $SD$  curve causes a coupled inward movement of the  $LC$  yield curve (see Equation 6). This coupled inward movement of the  $LC$  curve represents the reduced stability of the soil skeleton as meniscus water bridges are lost during a wetting process where voids are flooding with water (plastic increases of  $S_r$ ), meaning that reduced values of  $p^*$  are required to cause mechanical yielding. The coupled inward movement of the  $LC$  curve is not accompanied by plastic volumetric strains, because this would require direct yielding on the  $LC$  curve, which can only occur when the stress path reaches the  $LC$  curve.

After point  $Y_3$  on wetting path  $EF$ , the coupled inward movement of the  $LC$  yield curve predicted by the model occurs faster than the leftward movement of the stress point (i.e.  $p_0^*$  reduces proportionally faster than  $p^*$ ), so that the  $LC$  yield curve gradually moves closer to the stress point. In the example shown in Figure 2, yield point  $Y_4$  corresponds to the point where the  $LC$  yield curve reaches the stress point (the locations of the three yield curves at this point are shown by the chain dotted lines). From  $Y_4$  until the end of the wetting path at  $F$ , simultaneous yielding on  $SD$  and  $LC$  yield curves is occurring, with the stress point at the corner between the two yield curves. From  $Y_4$  to  $F$  the overall movement of the  $LC$  curve is the combination of a coupled inward movement (caused by the plastic increase of  $S_r$  associated with yielding on the  $SD$  curve) and a smaller component of direct outward movement caused by yielding on the  $LC$  curve. The yielding on the  $LC$  curve from point  $Y_4$  is accompanied by the occurrence of positive plastic volumetric strains, which will generally more than offset the simultaneous occurrence of small negative elastic volumetric strains. Point  $Y_4$  therefore corresponds to the onset of collapse compression during wetting.

It is important to note that yielding on the *LC* yield curve during wetting and the associated plastic compression are produced by a reduction of the mechanical yield stress  $p_o^*$ , caused by a reduction of the stabilizing effect of meniscus water bridges, as voids flood with water, and not by an increase of mean Bishop's stress  $p^*$  (indeed  $p^*$  actually reduces during wetting). Wetting-induced collapse compression is therefore associated in the model with simultaneous yielding on *SD* and *LC* curves. The model will not always predict collapse compression during wetting, because for some wetting stress paths the model predicts that a saturated condition is achieved before the *LC* yield curve reaches the stress point.

The descriptions above and the stress paths shown in Figure 2 illustrate how the model of Wheeler et al. (2003) is able to predict the occurrence of plastic compression during loading, drying and wetting paths and that in all three cases the occurrence of plastic volumetric strains corresponds to yielding on a single *LC* yield curve.

### **Simulation of an experimental test**

A practical demonstration of the ability of the model to predict accurately the occurrence and magnitude of plastic compression during loading, drying and wetting paths is provided here by presenting a simulation of an experimental test reported by Kato (1998) and Kato and Kawai (2000). This test on a compacted clay, in a suction controlled triaxial cell, involved only isotropic stress states and the applied stress path in the  $\bar{p}:s$  plane is shown in Figure 3. The test started with initial equalisation at point *A*, with  $\bar{p} = 20$  kPa and  $s = 49$  kPa (much lower than the previous as-compacted suction). The subsequent stress path involved a drying stage *AB* (at constant  $\bar{p} = 20$  kPa), a loading stage *BC* (at constant  $s = 245$  kPa) and a wetting stage *CD* (at constant  $\bar{p} = 196$  kPa) to  $s = 0$ .

Table 1 shows the values of the model parameters (soil constants) used for the simulation. These parameters are the gradients  $\lambda$  and  $\kappa$  of normal compression lines and swelling lines respectively (both defined in the  $e:\ln p^*$  plane from isotropic loading-unloading tests involving no plastic changes of degree of saturation, such as saturated tests), the gradients  $\lambda_s$  and  $\kappa_s$  of the main wetting/drying curves and scanning curves respectively (both defined in the  $S_r:\ln s^*$  plane from retention tests involving no plastic volumetric strains) and the two coupling parameters  $k_1$  and  $k_2$ . Complete

definitions of the model parameters and their calibration are given elsewhere (Lloret 2011; Lloret-Cabot et al. 2013).

Table 2 shows the initial state (representing point  $A$  in Figure 3) used for the simulation. Note that, in selecting initial values for the hardening parameters  $p_0^*$  and  $s_D^*$ , it was assumed that point  $A$  was at the corner between the  $LC$  and  $SD$  yield curves, because the experimental data from the previous equalisation stage indicated the occurrence of large (i.e. plastic) volumetric strains and large (i.e. plastic) changes of degree of saturation in wetting to point  $A$ . No initial value was selected for the hardening parameter  $s_I^*$  (defining the initial location of the  $SI$  yield curve), because the experimental data from test stages  $ABCD$  suggested that the  $SI$  yield curve was never reached (no occurrence of plastic decreases of  $S_r$ ) and hence it was not necessary to include the  $SI$  yield curve in the simulation.

Figures 4, 5 and 6 show the results of the model simulation together with the corresponding experimental data. In all the following figures, model simulations are identified by a heavy continuous line whereas experimental results are indicated by symbols joined by a finer line. The stress path in the  $p^* : s^*$  plane is shown in Figure 4, the variation of void ratio  $e$  is shown in Figure 5 (plotted against both  $\bar{p}$  and  $p^*$ ) and the variation of degree of saturation  $S_r$  is shown in Figure 6 (plotted against both  $s$  and  $s^*$ ).

In Figure 4, the initial positions of the  $LC$  and  $SD$  yield curves (at point  $A$ ) are indicated by  $LC_A$  and  $SD_A$  respectively, and the new positions of the yield curves corresponding to points  $B$ ,  $C$  and  $D$  are also indicated. Throughout drying path  $AB$ , yielding on only the  $LC$  yield curve is predicted, and at point  $B$  the stress point is still on the  $LC$  curve but no longer on the  $SD$  yield curve. During the early part of loading path  $BC$ , yielding on only the  $LC$  yield curve is predicted. However, this yielding on the  $LC$  curve produces coupled upward movement of the  $SD$  yield curve, which means that the corner between  $LC$  and  $SD$  yield curves is reached once more at point  $Y$ , and during the later part of the loading path (from  $Y$  to  $C$ ) simultaneous yielding on  $LC$  and  $SD$  curves is predicted. Throughout wetting path  $CD$  simultaneous yielding on  $LC$  and  $SD$  curves is predicted (even though  $p^*$  is reducing, yielding on the  $LC$  curve is required, in order to partially offset the coupled inward movement of the  $LC$  curve caused by yielding on the  $SD$  curve, as described earlier).

Figure 5 shows that the model simulation, which involves yielding on the  $LC$  curve throughout the

entire drying, loading and wetting stages, correctly predicts large magnitudes of compression during all three stages of the test. The model simulation provides an accurate match to the experimental variation of void ratio  $e$  in all test stages. A further aspect of validation of some of the concepts underlying the model is that when the variation of void ratio is plotted against  $p^*$  both experimental results and model simulation show no discontinuity of gradient at the transfer from drying stage  $AB$  to loading stage  $BC$  (it should be noted that the model only predicts this continuity of gradient between drying and loading stages when, as in this case, both the final part of one stage and the initial part of the next stage involve no yielding on  $SI$  or  $SD$  yield curves).

Figure 6 shows that the model simulation also provides an excellent match to the experimental variation of degree of saturation  $S_r$ . Very little change of  $S_r$  is predicted during drying stage  $AB$  (only a very small elastic decrease of  $S_r$ ), a modest increase of  $S_r$  is predicted during loading stage  $BC$  (dominated by a plastic decrease of  $S_r$  once the  $SD$  yield curve is reached at point  $Y$  in Figure 3) and a very large increase of  $S_r$  is predicted during wetting path  $CD$ .

The only significant mis-match between model simulation and experimental results is at the very end of wetting stage  $CD$ , where the model predicts achievement of a saturated condition whereas the experimental results show  $S_r$  achieving a final value of 0.94 (see Figure 6). This is probably because the wetting stage was performed too fast (only 24 hours for the full wetting stage) to maintain proper equalisation of pore air pressure throughout the sample once the air phase became discontinuous at very high degree of saturation (once this happens, the only way for air to continue to drain from the sample is by the very slow processes of dissolution and subsequent diffusion). Close inspection of the experimental variation of  $S_r$  in Figure 6 shows a discontinuity of gradient at the very end of wetting stage  $CD$ , which supports this interpretation. This would also explain why the experimental results in Figure 5 show a smaller compression than predicted by the model in this very last part of wetting stage  $CD$ .

## **Conclusion**

Within the coupled mechanical and water retention constitutive model of Wheeler et al. (2003), the occurrence of plastic compression during loading, drying and wetting stages have all been unified as essentially the same process of yielding on a single  $LC$  yield curve. This corresponds to slippage at

inter-particle or inter-aggregate contacts, when the applied value of mean Bishop's stress  $p^*$  reaches a yield value  $p_o^*$ . During loading or drying paths this yield condition is reached by  $p^*$  increasing. In contrast, during a wetting path the yield condition is reached as a consequence of a reduction of the yield stress  $p_o^*$ , due to a coupled inward movement of the  $LC$  curve produced by yielding on the  $SD$  yield curve (this represents a reduction in the stabilizing effect produced by meniscus water bridges as some meniscus water bridges are lost during flooding of voids with water).

Model predictions show excellent agreement with the experimental data from a test by Kato (1998), which involved large (plastic) compressions during successive drying, loading and wetting stages. The model was able to predict accurately not only the variation of void ratio (mechanical behaviour) but also the variation of degree of saturation (water retention behaviour), thus demonstrating the capabilities of the model. The simulation presented in this paper did not investigate model performance during drying paths involving plastic decreases of degree of saturation.

## Acknowledgements

The work presented here benefited from a SYNERGY scholarship between the Universities of Strathclyde and Glasgow and also from a MacRobertson Scholarship from the University of Glasgow.

## References

- Alonso, E.E., Gens, A. and Hight, D.W. 1987. Special problem soils: general report. *In* Proceedings of the 9<sup>th</sup> European Conference on Soil Mechanics and Foundation Engineering, Dublin. Vol. 3, pp. 1087-1146.
- Alonso, E.E., Gens, A. and Josa, A. 1990. A constitutive model for partially saturated soils. *Géotechnique*, **40**(3): 405-430.
- Houlsby, G.T. 1997. The work input to an unsaturated granular material. *Géotechnique*, **47**(1): 193-196.
- Kato, S. 1998. Deformation characteristics of a compacted clay in collapse under isotropic stress state and its shear deformation after collapse. *Journal of the Japan Society of Civil Engineers*, 596/III-43: 271-281 (in Japanese).
- Kato, S. and Kawai, K. 2000. Deformation characteristics of a compacted clay in collapse under isotropic and triaxial stress state. *Soils and Foundations*, **40**(5): 75-90.
- Lloret, M. 2011. Numerical modelling of coupled behaviour in unsaturated soils, Ph.D. Thesis, University of Strathclyde and University of Glasgow, United Kingdom.

- Lloret-Cabot, M., Sánchez, M. and Wheeler, S.J. 2013. Formulation of a 3D constitutive model for unsaturated soils incorporating mechanical-water retention couplings. *International Journal for Numerical and Analytical Methods in Geomechanics*. doi:10.1002/nag.2176.
- Wheeler, S.J., Sharma, R.S. and Buisson, M.S.R. 2003. Coupling of hydraulic hysteresis and stress-strain behaviour in unsaturated soils. *Géotechnique*, **53**(1): 41-54.

**Table 1. Model parameter values for simulation of test of Kato (1998)**

<b>Parameter</b>	<b>Value</b>
$\lambda$	0.067
$\kappa$	0.002
$\lambda_s$	0.070
$\kappa_s$	0.001
$k_1$	0.46
$k_2$	0.89

**Table 2. Initial state for simulation of test of Kato (1998)**

<b>Variable</b>	<b>Value</b>
<i>Mean net stress (<math>\bar{p}</math>)</i>	20 kPa
<i>Matric suction (<math>s</math>)</i>	49 kPa
<i>Void ratio (<math>e</math>)</i>	1.261
<i>Degree of saturation (<math>S_r</math>)</i>	0.543
<i>Modified suction (<math>s^*</math>)</i>	27.32 kPa
<i>Mean Bishop's stress (<math>p^*</math>)</i>	46.6 kPa
<i>Hardening parameter for LC (<math>p_0^*</math>)</i>	46.6 kPa
<i>Hardening parameter for SD (<math>s_D^*</math>)</i>	27.32 kPa

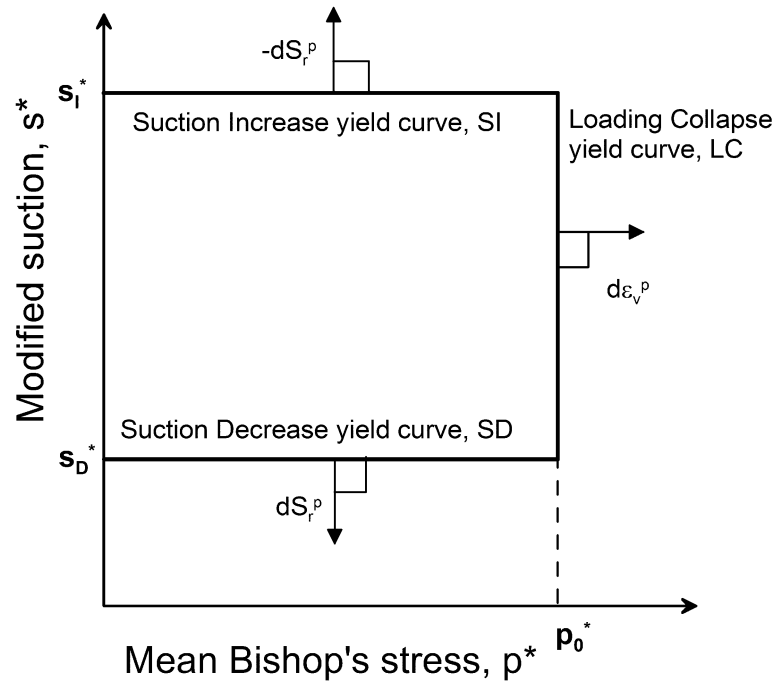


Fig. 1. Yield curves for isotropic stress states (Wheeler et al., 2003)

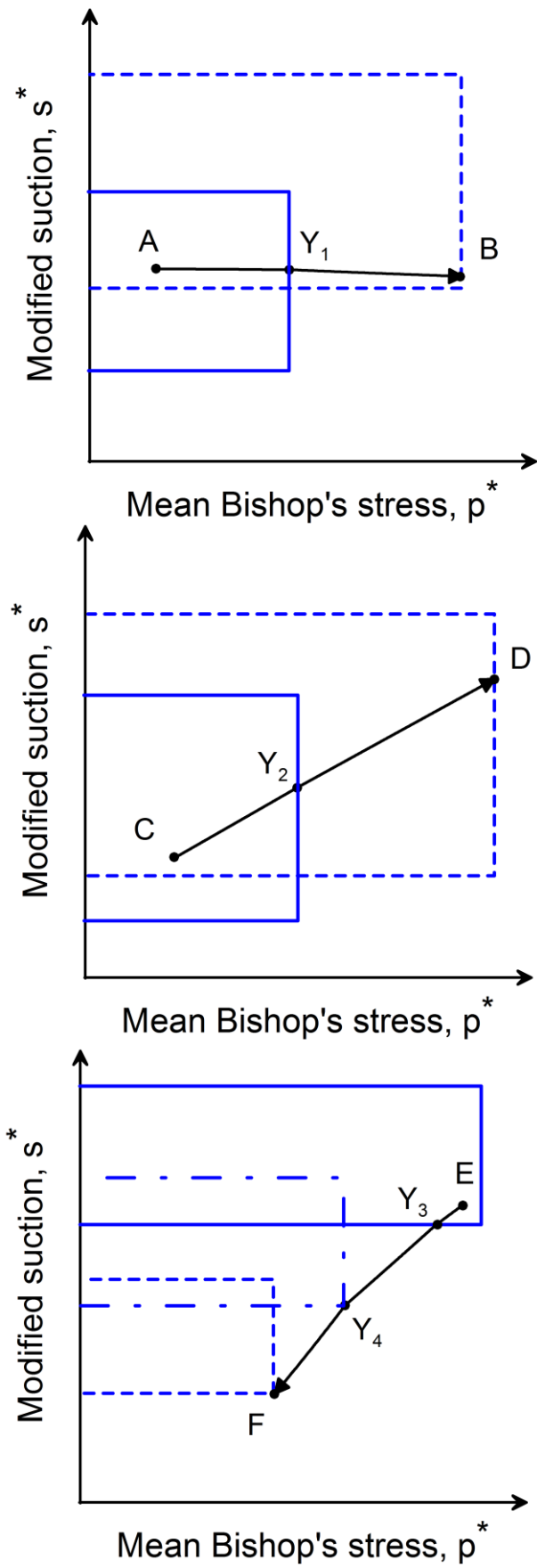


Fig. 2. Prediction of plastic compression during loading, drying and wetting

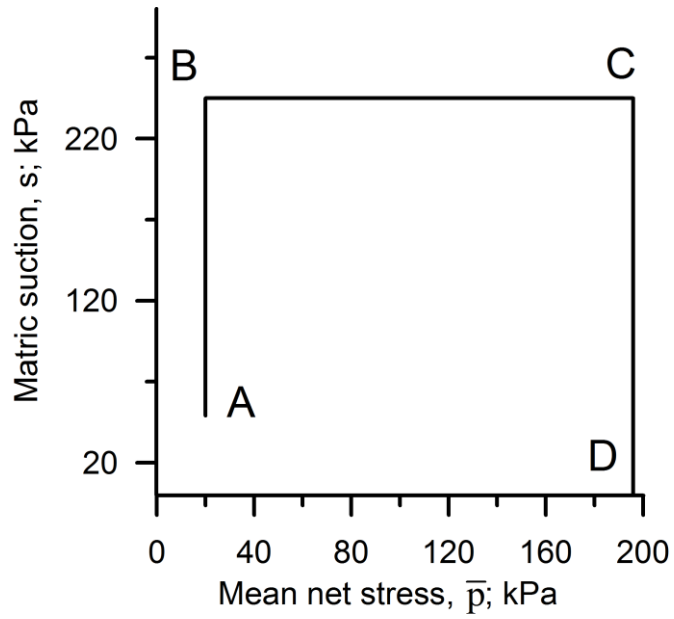


Fig. 3. Applied stress path for the experimental test of Kato (1998).

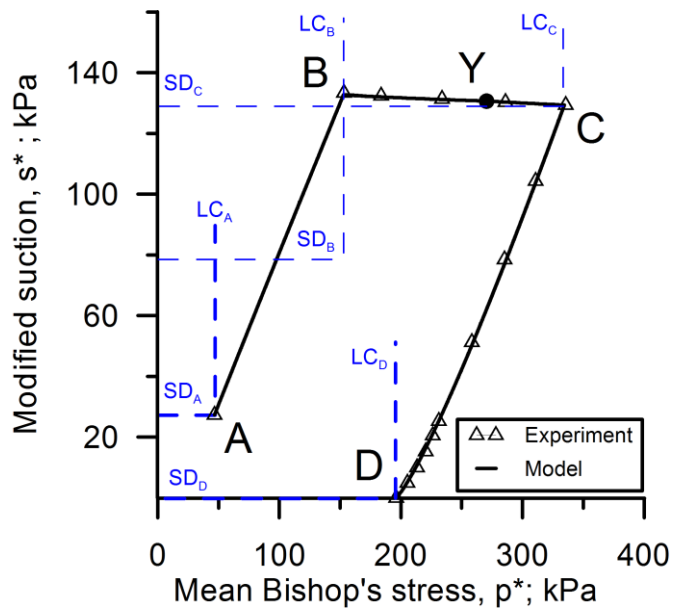


Fig. 4. Comparison of model simulation and experimental results: stress path in  $p^* : s^*$  plane

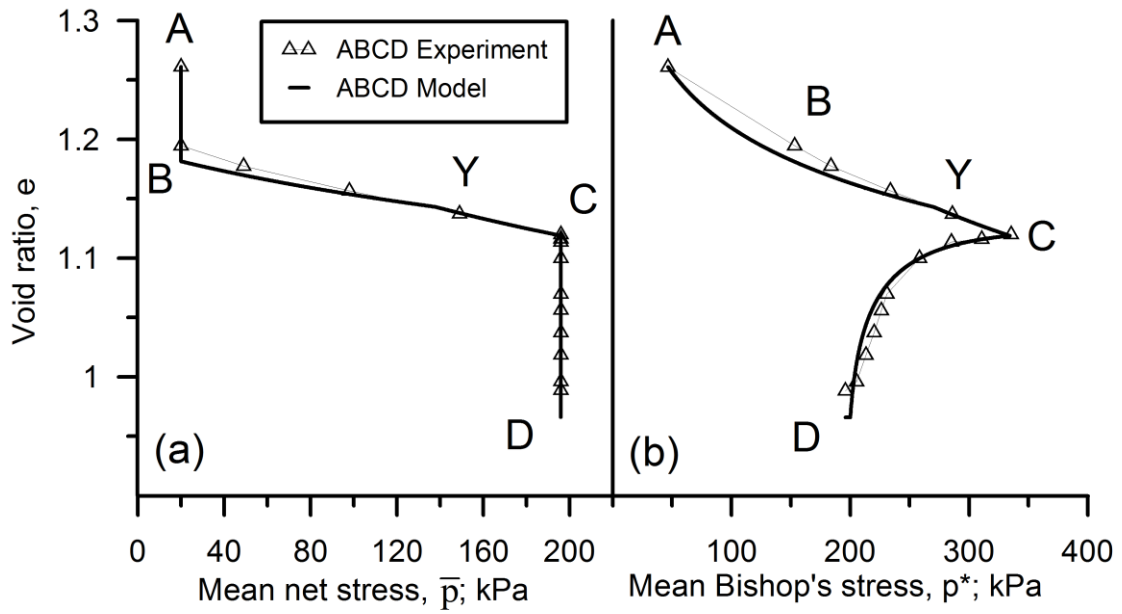


Fig. 5. Comparison of model simulation and experimental results: variation of void ratio

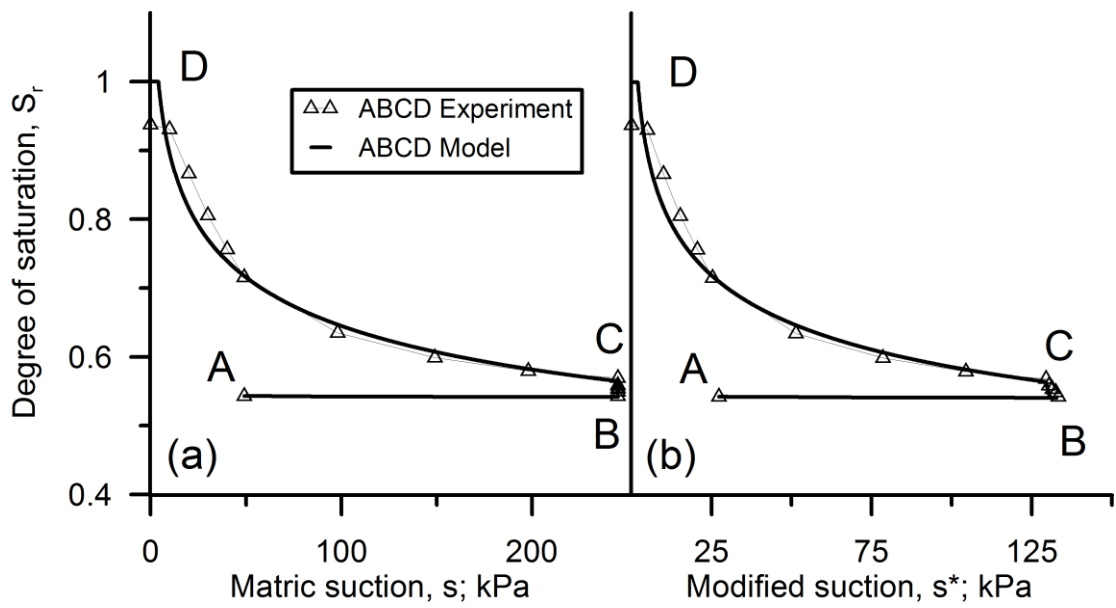


Fig. 6. Comparison of model simulations and experimental results: variation of degree of saturation